AFRL-SN-RS-TR-2000-150
Final Technical Report
October 2000

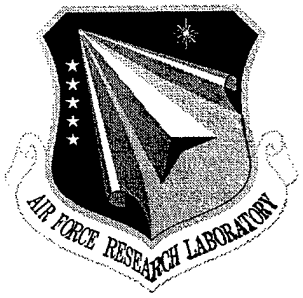


# PHOTONICS CIRCUITS TECHNOLOGY FOR RF PHOTONICS SYSTEMS

**The Regents of the University of California**

**Sponsored by**
**Defense Advanced Research Projects Agency**
**DARPA Order No. E392**

*APPROVED FOR PUBLIC RELEASE; DISTRIBUTION UNLIMITED.*



**AIR FORCE RESEARCH LABORATORY**
**SENSORS DIRECTORATE**
**ROME RESEARCH SITE**
**ROME, NEW YORK**

This report has been reviewed by the Air Force Research Laboratory, Information Directorate, Public Affairs Office (IFOIPA) and is releasable to the National Technical Information Service (NTIS). At NTIS it will be releasable to the general public, including foreign nations.

AFRL-SN-RS-TR-2000-150 has been reviewed and is approved for publication.

APPROVED: James R. Hunter

JAMES R. HUNTER
Project Engineer

FOR THE DIRECTOR: Robert G. Polce

ROBERT G. POLCE, Chief
Rome Operations Office
Information Directorate

If your address has changed or if you wish to be removed from the Air Force Research Laboratory Rome Research Site mailing list, or if the addressee is no longer employed by your organization, please notify AFRL/SNDP, 25 Electronic Pky, Rome, NY 13441-4515. This will assist us in maintaining a current mailing list.

Do not return copies of this report unless contractual obligations or notices on a specific document require that it be returned.

# PHOTONICS CIRCUITS TECHNOLOGY FOR RF PHOTONICS SYSTEMS

Paul K. L. Yu, S. S. Lau, W. X. Chen,
A. R. Clawson, G. L. Li, Q. Z. Liu,
D. S. Shin, Yang Wu, Q. J. Xing and J. T. Zhu

Contractor: The Regents of the University of California
Contract Number: F30602-97-C-0018
Effective Date of Contract: 27 November 1996
Contract Expiration Date: 26 November 1999
Program Code Number: 6L10
Short Title of Work: Photonics Circuits Technology for RF Photonics Systems
Period of Work Covered: Nov 96 - Nov 99

Principal Investigator: Paul K. L. Yu
Phone: (619) 534-6180
AFRL Project Engineer: James R. Hunter
Phone: (315) 330-7045



This research was supported by the Defense Advanced Research Projects Agency of the Department of Defense and was monitored by James R. Hunter, AFRL/SNDP, 25 Electronic Pky, Rome, NY.

# REPORT DOCUMENTATION PAGE

*Form Approved*
*OMB No. 0704-0188*



| 1. AGENCY USE ONLY *(Leave blank)* | 2. REPORT DATE | 3. REPORT TYPE AND DATES COVERED |
|---|---|---|
| | OCTOBER 2000 | Final Nov 96 - Nov 99 |

**4. TITLE AND SUBTITLE**
PHOTONICS CIRCUITS TECHNOLOGY FOR RF PHOTONICS SYSTEMS

**5. FUNDING NUMBERS**
C - F30602-97-C-0018
PE - 63765E, 63226E
PR - E392
TA - 00
WU - 01

**6. AUTHOR(S)**
Paul K. L. Yu, S. S. Lau, W. X. Chen, A. R. Clawson, G. L. Li, Q. Z. Liu, D. S. Shin, Yang Wu, Q. J. Xing and J. T. Zhu

**7. PERFORMING ORGANIZATION NAME(S) AND ADDRESS(ES)**
The Regents of the University of California, San Diego
Contract and Grant Administration - 0934
La Jolla CA 92093-0934

**8. PERFORMING ORGANIZATION REPORT NUMBER**
N/A

**9. SPONSORING/MONITORING AGENCY NAME(S) AND ADDRESS(ES)**
Defense Advanced Research Projects Agency
3701 N. Fairfax Drive
Arlington VA 22060-6218

Air Force Research Laboratory/SNDP
25 Electronic Pky
Rome NY 13441-4514

**10. SPONSORING/MONITORING AGENCY REPORT NUMBER**
AFRL-SN-RS-TR-2000-150

**11. SUPPLEMENTARY NOTES**
Air Force Research Laboratory Project Engineer: James R. Hunter/SNDP/(315) 330-7045

**12a. DISTRIBUTION AVAILABILITY STATEMENT**
APPROVED FOR PUBLIC RELEASE; DISTRIBUTION UNLIMITED.

**12b. DISTRIBUTION CODE**

**13. ABSTRACT** *(Maximum 200 words)*

Optical transmission of analog RF signals is potentially useful in a number of applications including RF distribution systems. Such systems can be used in commercial CATV and wireless communications and in military communication and radar systems. With compatible components used at transmitters and receivers, analog fiber optic links suffer much less performance degradation than conventional coaxial cable links as the system bandwidth increases. In the first year program we studied large Optical Cavity waveguide modulator design and demonstrated a low optical insertion loss waveguide modulator at 1.34 microns wavelength (as low as 8 dB w/o AR coating). This design is based upon the matching of the mode profile of the fiber and the modulator waveguides. The design is extended to 1.55 microns wavelength. We also demonstrated a novel scheme of bias-tracking of the electroabsorption waveguide modulator. The scheme is based upon the photocurrent generated at the modulator. Effective tracking is obtained as the polarization, wavelength (or ambient temperature), and power of the input light are varied. Experimental evidence was obtained for a combined Franz-Keldysh effect and Quantum Confined Stark Effect modulator for a large multi-octave spurious free dynamic range. Low loss planar photoelastic waveguide on both InP and GaAs substrates was achieved.

**14. SUBJECT TERMS**
Optical Modulator, Optical Waveguide Modulator, Electroabsorption Modulator, RF Photonic Links

**15. NUMBER OF PAGES**
44

**16. PRICE CODE**

| 17. SECURITY CLASSIFICATION OF REPORT | 18. SECURITY CLASSIFICATION OF THIS PAGE | 19. SECURITY CLASSIFICATION OF ABSTRACT | 20. LIMITATION OF ABSTRACT |
|---|---|---|---|
| UNCLASSIFIED | UNCLASSIFIED | UNCLASSIFIED | UL |

## TABLE OF CONTENTS

## LIST OF FIGURES



## LIST OF TABLES

## Summary of Accomplishments

1. In the option year program we have investigated some of the critical design and fabrication issues for achieving traveling wave electroabsorption waveguide modulator with electrical bandwidths well beyond 50 GHz. Device fabrication is carried out for the high frequency designs.
2. We extended the bias-tracking of the electroabsorption waveguide modulator studied in the first year. In this alternative scheme, the harmonics of the AC photocurrent generated at the modulator is used for dynamic self-bias control of electroabsorption modulators. Effective tracking is obtained as the polarization, wavelength (or ambient temperature), and power of the input light are varied.
3. We have developed a concise RF equivalent circuit model for analyzing the electroabsorption modulators. With this model, circuit parameters extracted from measured $S_{11}$ values for an MQW EAM are used to estimate the modulator E/O responses, and are found consistent with measured responses. The model clarifies the effect of optical power to the EAM impedance and modulation bandwidth.
4. We demonstrated an integrated EA waveguide/mixer for frequency conversion of RF signals that utilize the electric-field-controlled absorption in an electroabsorption (EA) waveguide. Applying this approach to an InAsP/GaInP multiple-quantum-well EA waveguide, a conversion loss of 18.4 dB is obtained at 10-mW optical local oscillator power, and a sub-octave, two-tone spur-free dynamic range of 120.0 dB-$Hz^{4/5}$ is measured for an up-converted signal at 1.9 GHz.

## DETAILED TECHNICAL ACHIEVEMENT ON EFFORT

The optical transmission of analog RF signals is potentially useful in a number of applications including RF distribution systems. Such systems can be used in commercial CATV and wireless communications, and in various military communication and radar systems. With compatible components used at transmitters and receivers, analog fiber

optics links suffer much less performance degradation than conventional coaxial cable links as the system bandwidth increases.

In the first year program (1) we studied large Optical Cavity waveguide modulator design, and demonstrated a low optical insertion loss waveguide modulator at 1.34 μm wavelength (as low as 8 dB without AR coating). This design is based upon the matching of the mode profile of the fiber and the modulator waveguides. The design is extended to 1.55 μm wavelength. (2) We also demonstrated a novel scheme of bias-tracking of the electroabsorption waveguide modulator. The scheme is based upon the photocurrent generated at the modulator. Effective tracking is obtained as the polarization, wavelength (or ambient temperature), and power of the input light are varied. (3) We obtained experimental evidence for a combined Franz-Keldysh effect and Quantum Confined Stark Effect modulator for a large multi-octave spurious free dynamic range. (4) We have achieved low loss planar photoelastic waveguide on both InP and GaAs substrates.

The following describes the main results obtained in the option year program.

## A. Investigation of the Traveling wave Electroabsorption Waveguide Modulator

Semiconductor electroabsorption modulator (EAM) is a promising alternative to lithium niobate electro-optic modulator (EOM) for use in analog high-speed fiber optic links due to its inherent small size, high modulation efficiency, and potential for monolithic integration with other electronic and optoelectronic components. An attractive feature of the EAM is its relative ease to achieve a large bandwidth with a short lumped element waveguide. A 50 GHz bandwidth modulator has been reported with a 63 μm long waveguide [1]. However, to achieve a larger bandwidth using the lumped element approach, one has to further shorten the modulator waveguide to overcome the RC time limit of the device. Unfortunately, this approach reduces the modulation efficiency due to the shorter interaction length. This is most critical in analog operation where RF link loss and noise figure must be minimized. To overcome the RC bandwidth limit and to avoid significantly compromising the modulation efficiency, the traveling wave electroabsorption modulator (TW-EAM) has been proposed and experimentally

investigated by several groups [2,3] In this program, some of the critical design and fabrication issues for achieving TW-EAM electrical bandwidths well beyond 50 GHz are investigated. Device fabrication is carried out for some of the designs.

The essential requirements for achieving a traveling wave modulator include: (1) The modulator electrode must be designed as a transmission line to distribute the capacitance over the entire length of the line, (2) the microwave and modulated light should propagate at the same velocity so that the microwave signal is always enhancing the modulation depth during propagation, (3) only forward-going propagating microwave and optical waves exist in the waveguide, (4) low microwave attenuation and optical propagation loss must be achieved in order to achieve high modulation efficiency at high frequency. Since the microwave attenuation of the electrode increases with frequency, both bandwidth and modulation efficiency at high frequency are compromised. Optical propagation loss also reduces the modulation efficiency, albeit it has little impact on the bandwidth. These detrimental effects can be minimized by device designs that have very low microwave attenuation and optical propagation loss.

For a conventional EAM waveguide, the microwave impedance is much less than the standard 50 Ω input transmission line, the microwave phase velocity is much smaller than the optical group velocity, and microwave and optical attenuation always exist. Furthermore, all microwave properties of the EAM waveguide are frequency dependent, and the waveguide impedance has an imaginary or lossy component. Consequently, it is very difficult to achieve perfect impedance matching and velocity matching for the TW-EAM and to completely eliminate the attenuation loss. This compounds the difficulty in producing an ultra high-speed TW-EAM with high modulation efficiency.

In this program, some practical and simple approaches for producing a TW-EAM with an electrical bandwidth beyond 50 GHz are examined. Effects of impedance mismatch, velocity mismatch and microwave attenuation on the modulator frequency response are investigated. A guideline for the TW-EAM design is established. Due to the present optical propagation loss encountered in the EAM, the resulting modulator is found to be restricted to a rather short waveguide length. A quasi-static equivalent circuit model is employed to estimate the frequency dependent microwave properties of a

standard EAM waveguide. This circuit model includes the effect of photocurrent generation.

***Modulator Frequency Response:*** With small signal modulation, the modulation efficiency of a TW-EAM can be derived to be proportional to $\left|\int_0^L V_{ac}(x)dx\right|^2$, in which $V_{ac}(x)$ is the modulation voltage for an optical wave packet in TW-EAM at position x, L is the total modulation length. $V_{ac}(x)$ can be calculated with considering the possibility of multiple microwave reflections inside the modulator. For an analog fiber optic link using the TW-EAM, the RF gain in the general case can be normalized with respect to the ideal case, in which the impedance matching and velocity matching are perfect and microwave loss is zero. Consequently, the normalized RF link gain, including effects of impedance mismatch, velocity mismatch and microwave attenuation, can be expressed as:

$$G_{NORM} = \left| \frac{T}{1-\Gamma_L\Gamma_S \exp(-2\gamma_\mu L)} \left\{ \frac{\exp\{(j\beta_o - \gamma_\mu)L\}-1}{(j\beta_o - \gamma_\mu)L} + \Gamma_L \exp(-2\gamma_\mu L) \frac{\exp\{(j\beta_o + \gamma_\mu)L\}-1}{(j\beta_o + \gamma_\mu)L} \right\} \right|^2 . \quad (1)$$

where T is the microwave amplitude transmission coefficient at the modulator source port (x=0), $\Gamma_S$ and $\Gamma_L$ are the modulator (internal) reflection coefficients at the source and load ports, respectively, and $\gamma_\mu = \alpha_\mu + i\beta_\mu$ is the microwave propagation constant ($\alpha_\mu$ is the microwave attenuation factor and is frequency dependent. $\beta_\mu = \omega/\upsilon_\mu$ is the wave number associated with the microwave frequency $\omega$ and the microwave phase velocity $\upsilon_\mu$). $\beta_o = \omega/\upsilon_o$, where $\upsilon_o$ is the optical group velocity. With $Z_S$, $Z_m$ and $Z_L$ defined as the characteristic microwave impedance of the source transmission line, the modulator and the terminator, respectively, the following relations are obtained:

$$\Gamma_S = \frac{Z_S - Z_m}{Z_S + Z_m}, \qquad \Gamma_L = \frac{Z_L - Z_m}{Z_L + Z_m}, \qquad T = \frac{2Z_m}{Z_S + Z_m} = 1 - \Gamma_S . \quad (2)$$

***Microwave Properties of the TW-EAM Waveguide:*** The TW-EAM impedance $Z_m$ and velocity $\upsilon_\mu$ and microwave attenuation $\alpha_\mu$ can be estimated with a quasi-static circuit model for a unit length of TW-EAM transmission line, which is shown in Figure 1(a). In this circuit diagram, $R_{con}$ is the conduction resistance, $L_m$ is the inductance, $R_S$ is the device series resistance, $C_m$ is the junction capacitance, $R_J$ is the junction leakage

resistance, $I_O$ is the photocurrent governed by electroabsorption, and $C_P$ is the parasitic capacitance. For well designed EAMs, $C_P$ is typically very small in value and $R_J$ is much larger than the impedance governed by $C_m$ for microwave frequencies beyond 1 GHz. Therefore, both $C_P$ and $R_J$ can be replaced by an electrical open. With these assumptions, the circuit model can be approximated by that shown in Figure 1(b), where $R_O = dI_O/dV_J$ is the equivalent ac resistance due to the dependence of the current $I_O$ on the modulator junction voltage $V_J$. This optical power dependent current path can significantly alter the microwave properties of the TW-EAM at high input optical power where RF link gain is high.

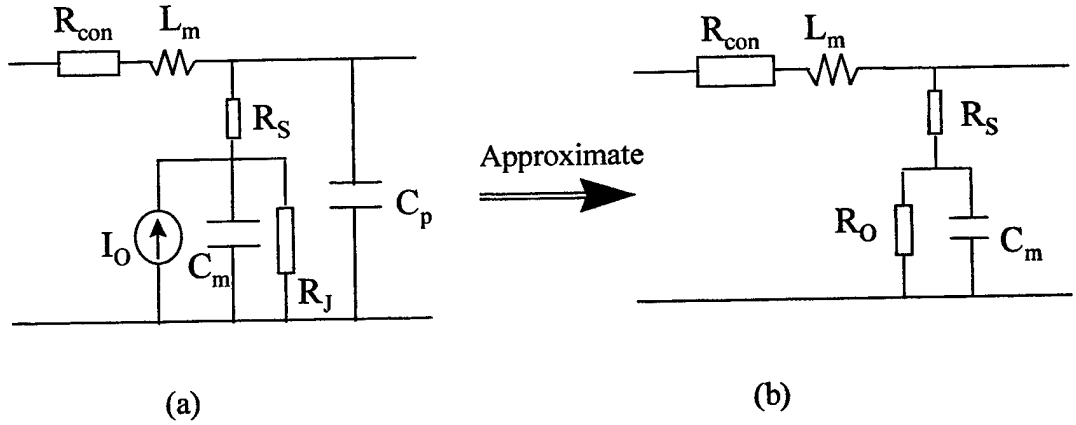


*Figure 1. Quasi-static circuit model for a unit length of TW-EAM transmission line.*

Using the circuit parameters in Figure 1(b), all of the relevant microwave properties of TW-EAM waveguide can be derived by:

$$Z_m = \sqrt{(R_{con} + j\omega L_m)\{R_S + R_O/(1 + j\omega R_O C_m)\}} \quad (3)$$

$$\gamma_\mu = \alpha_\mu + j\beta_\mu = \sqrt{(R_{con} + j\omega L_m)/\{R_S + R_O/(1 + j\omega R_O C_m)\}} \quad (4)$$

The circuit parameters of the TW-EAM waveguide transmission line are generally frequency dependent. However, in the high frequency region above 1 GHz where all the skin, edge and proximity effects are fully pronounced, $L_m$, $C_m$, $R_S$ and $R_O$ tend to constants, and $R_{con}$ increases as the square root of frequency. To estimate the values of circuit parameters above 1 GHz, experimental results have to be used. Measurements of microwave properties have been reported for EAMs and EOMs fabricated on InP

substrates with planar-microstrip p-i-n structures. At high frequencies, Eq. (3) and (4) can be significantly simplified. So that the measured high frequency $Z_m$ and $\gamma_\mu$ can be used to estimate $L_m$ and $C_m$ and $R_{con}$ for their respective structures. These values in turn can be used to estimate the circuit parameters for a standard InGaAsP/InP EAM with the waveguide width w~3 μm and the intrinsic layer thickness $d_I$~0.3 μm. Taking $R_{con} \propto w^{-1}$ and $C_m \propto w/d_I$, it can be inferred that $C_m$~1.2 pF/mm and $R_{con}$~6 $\Omega mm^{-1}GHz^{-1/2}$ for the standard EAM. However, $L_m$ may depend on various electrode and waveguide layer parameters. For the standard EAM, $L_m$ can vary significantly but will fall into the wide inductance range of 0.1 to 1 nH/mm.

For the standard EAM, $R_S$~1 Ωmm is a reasonable value. $R_O$ is optical power dependent. At low optical power, $R_O$ is simply an open circuit; at high optical power, $R_O$ becomes smaller in value so that it can no longer be considered an open circuit. For example, at 5 dBm input optical power, $dI_O/dV_J$ can be ~0.45 mA/V for a 180 μm long waveguide implying an $R_O$ of 400 Ωmm. At higher optical power and/or with a more efficient modulator, $R_O$ could be smaller than 20 Ωmm.

Consequently, frequency dependent microwave properties for the standard EAM waveguide can be obtained by substituting $L_m$, $C_m$, $R_{con}$, $R_S$ and $R_O$ into Eqs. (3) and (4). Due to the microwave voltage drop across $R_S$, the normalized link gain has to be modified as:

$$LG_{NORM} = G_{NORM} \frac{R_O^2}{\left|R_O + (1 + j\omega C_m R_O)R_S\right|^2} \tag{5}$$

with $G_{NORM}$ given by Eq. (1).

***Optimal Modulator Length for maximum RF link gain:*** It is often desirable to lengthen the modulator as much as possible to increase the modulation efficiency. However, there is an up limit due to the optical propagation loss. Consider a TW-EAM with perfect velocity matching and perfect impedance matching and no microwave loss. In this case, the modulation voltage $V_{ac}(x)$ for a particular optical wave packet is constant ($V_0$) along the whole waveguide. The modulated optical power can be expressed as:

$$I_{ac} = -I_{in}C^2 \exp(-\alpha_o L - \gamma\alpha_b L)\gamma \frac{d\alpha_b}{dV_b} V_0 L \,. \qquad (6)$$

where $I_{in}$ is the input optical power, C is the optical loss factor at each modulator facet, $\alpha_o$ is the optical propagation loss coefficient inside the modulator at zero bias voltage, $\gamma$ is the optical confinement factor in the modulator absorption layer, $\alpha_b$ is the absorption change due to the modulator DC bias $V_b$.

With larger L, the optimal DC bias voltage $V_b$ becomes smaller allowing $\alpha_b$ to be smaller. For EAMs, the optimal bias point $V_b$ usually results in a normalized transmission ($T = \exp(-\gamma\alpha_b L)$) value of 0.5 ~ 0.7. This implies that the term $\exp(-\gamma\alpha_b L)$ in Eq. (6) has little dependence on L. The dependence of $d\alpha_b/dV_b$ on L is difficult to model analytically. Usually, $d\alpha_b/dV_b$ is smaller for smaller $V_b$ as L increases. In Eq. (6), the most important terms are L and $\exp(-\alpha_o L)$. For a typical EAM with a 3 ~ 4 μm waveguide width and a 0.3 ~ 0.4 μm thick undoped absorption layer, the optical propagation loss ranges from 15 dB/mm to 20 dB/mm [1,5]. Most of the propagation loss comes from the residual absorption at zero bias.

To determine the optimal modulator length L for maximum RF link gain, first consider the L for maximizing $L\cdot\exp(-\alpha_o L)$ in Eq. (6). It can be calculated that for 15 dB/mm optical propagation loss the optimal L is ~0.3 mm, while for 20 dB/mm propagation loss the optimal L is ~0.22 mm. Owing to the fact that $d\alpha_b/dV_b$ is smaller for longer L, it will take an optimal length smaller than the above values to maximize the RF link gain. In Ref. [6], the optimal modulator length was measured to be 0.17 mm. A longer modulator length will not improve either the RF gain or the bandwidth.

***TW-EAM Approaches:*** For a typical EAM waveguide, all microwave properties are frequency dependent, microwave attenuation is pretty large, waveguide impedance is far from 50 Ω and has an imaginary part, and the microwave phase index ranges from 10 to 6. There are currently no published reports regarding the optical group index in InP/InGaAsP waveguides. However, the optical group index in a GaAs/AlGaAs waveguide has been measured to be ~3.73, which is larger than the optical phase index of 3.38. For a typical InP/InGaAsP waveguide, whose optical phase index is 3.2~3.3, an

optical group index of 3.5 is assumed. This implies a large velocity mismatch for standard 1.3 or 1.55 μm EAMs. Consequently, it may be difficult to achieve a large bandwidth for a TW-EAM with a conventional EAM waveguide with a typical electrode design.

A simple way to achieve a large TW-EAM bandwidth is to use standard EAM waveguide matching with a low impedance terminator. This is similar to using a small shunt resistance in a lumped element EAM to broaden the bandwidth. For the standard EAM waveguide, it has been shown that $L_m$=0.1 to 1 nH/mm, $C_m$=1.2 pF/mm, $R_{con}$=6 $\Omega mm^{-1}GHz^{-1/2}$, $R_S$=1 Ωmm, $R_O$=$10^6$ Ωmm, L=0.2 mm and $R_S$=50 Ω. The calculated modulator frequency responses are shown in Figure 2(a). It is found that with $Z_L$=50 Ω for TW-EAM and $R_{sh}$=50 Ω for lumped element device, their frequency responses are very close. They both have approximately 22 GHz bandwidth. However, when $R_{sh}$ and $Z_L$ are reduced to 20 Ω, the TW-EAM has significantly better performance than the lumped element EAM. In this case, the TW-EAM has a bandwidth of about 50 GHz, whereas the lumped element EAM has only 33 GHz bandwidth.

With intrinsic absorption layer thickness is increased to 0.5 μm, $C_m$ will decrease to ~0.72 pF/mm. In this case with $Z_L$=22 Ω, the TW-EAM bandwidth will be extended to more than 90 GHz, whereas the lumped element EAM with the same structure only has 50 GHz bandwidth with $R_{sh}$=22 Ω . This is shown in Figure 2(b).

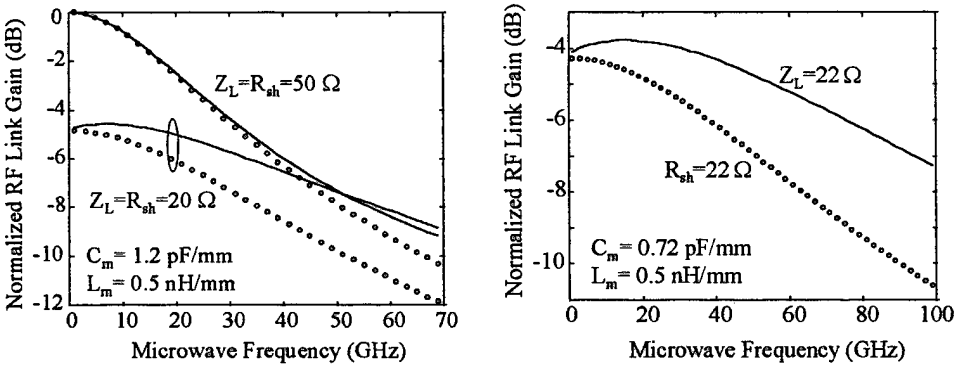


*Fig. 2. Comparisons between TW-EAM (solid lines) and lumped element EAM (symbol lines) with low impedance termination.*

The effect of waveguide inductance on TW-EAM bandwidth is investigated in Figure 3(a). When $Z_L$>50 Ω, the waveguide inductance has little impact on TW-EAM bandwidth. However, When $Z_L$=20 Ω, in the $L_m$ range of 0.1 nH/mm to 1 nH/mm, larger $L_m$ will yield larger bandwidth. Figure 3(b) shows that when high optical power causes $R_O$ to drop to 20 Ωmm, the TW-EAM low frequency gain drops 1.5 dB, but the bandwidth increases from 50 GHz to above 60 GHz. This is because at lower frequency, $1/\omega C_m$ is large compared with $R_O$, so that the AC photocurrent through $R_O$ is larger causing larger microwave loss. This flattens the TW-EAM frequency response and increases the bandwidth. Even though $R_O$ is not constant throughout the waveguide due to the fact that the absorbed optical power decays exponentially along the waveguide, it can be expected that the TW-EAM bandwidth will not be reduced by the large photocurrent.

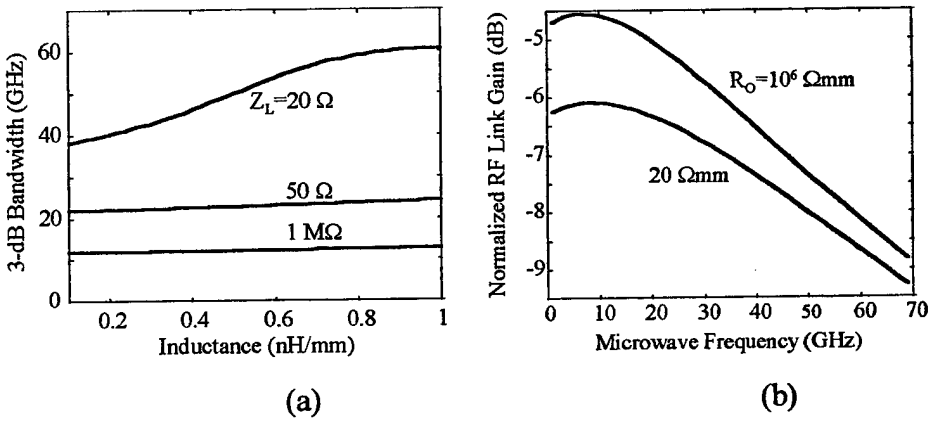


*Fig. 3. Effects of (a) waveguide inductance, (b) high optical power on TW-EAM performance.*

The TW-EAM frequency responses using various terminators have also been investigated. It shows that with a smaller impedance terminator, the TW-EAM bandwidth will be increased, whereas the low frequency RF gain will be sacrificed. The overall gain and bandwidth product is smaller with lower impedance terminator.

## B. Harmonic Signals from Electroabsorption Modulators for Bias Control

As noted in the first year program, the optimum bias of an electroabsorption waveguide modulator needs to be adjusted during operation, as the modulator transfer characteristics can change in response to changes in ambient temperature, polarization and optical power levels. To simplify the optical configuration for EAM bias control, we demonstrated in the first year program a self-bias control approach based upon the correlation between the RF link gain and the modulator DC photocurrent. In the option year program, we propose and demonstrate an alternative self-bias approach based upon the correlation between the RF link gain and the second harmonic signal reflected from the EAM. From the measured RF link gain and the EAM harmonic signal as a function of modulator bias, we show that the second harmonic exhibited a dip at a bias close to that for maximum RF link gain, as the optical power was varied from 8 to 14 dBm. These measurement results can be explained using an equivalent circuit model for the EAM, an extended circuit model in described in Section C. The observed correlation between the RF link gain and the second harmonic signal is mainly caused by the inherent electroabsorption effect in the modulator.

***Experiment:*** A fiber-packaged InGaAsP/InP Franz-Keldysh effect waveguide modulator is used in this work. The waveguide is 2.5 μm wide at the top and is 300 μm long. It has a 0.3 μm thick intrinsic InGaAsP ($\lambda_g$ = 1.24 μm) electroabsorption layer. To facilitate coupling to lensed fibers, a large optical cavity is incorporated in the waveguide. At 1.32 μm wavelength, the packaged device has a fiber-to-fiber optical insertion loss of 10.7 dB at zero bias.

Figure 4 depicts the measurement set-up, with arrows indicating the direction of signal flow. Two RF spectrum analyzers are used to simultaneously measure and display the EAM second harmonic signal, $P_{mod2}$, and the photodetector fundamental signal, $P_{det1}$. The RF source is set at 1 GHz and –20 dBm.

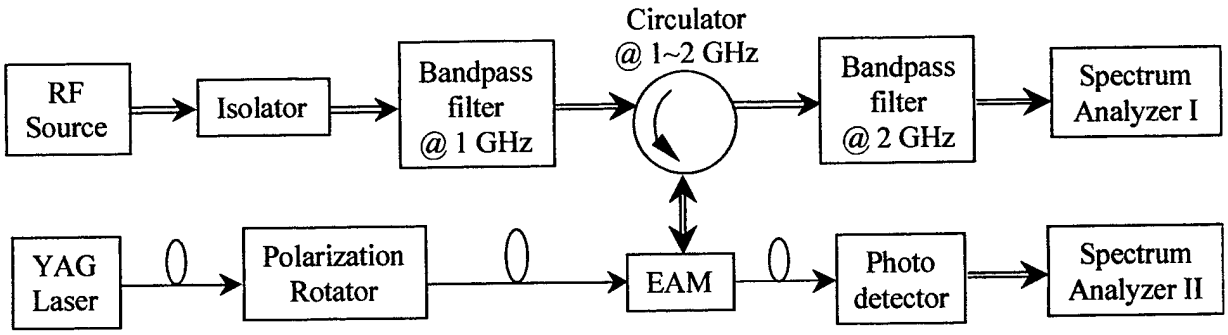


*Fig.4. Schematic diagram of measurement set-up. Two spectrum analyzers are used for measuring the EAM second order harmonic signals and the detector fundamental signals, respectively*

With the EAM biased at - 3.2 V, $P_{det1}$ is measured as a function of optical input power $P_{opt}$. For small $P_{opt}$, $P_{det1}$ versus $P_{opt}$ curve is a straight line in the logarithmic scale, with a slope of 2 dB/dB. When $P_{opt}$ is increased to 14 dBm, $P_{det1}$ is compressed by 1 dB from the line. Next, $P_{det1}$ and $P_{mod2}$ are measured as a function of modulator bias $V_m$, with $P_{opt}$ ranged from 0 to 14 dBm. Figures 5 show the measured $P_{det1}$ and $P_{mod2}$ versus $V_m$ curves at different $P_{opt}$'s. Within the measured $P_{opt}$ range, $P_{det1}$ always peaks at a certain voltage, denoted as $V_{RF\text{-}max}$. When $P_{opt}$ is large enough, $P_{mod2}$ exhibits a dip at a voltage denoted as $V_{m2\text{-}min}$. Table 1 lists the $P_{opt}$ and corresponding measured $V_{RF\text{-}max}$ and $V_{m2\text{-}min}$. Within the $P_{opt}$ range of 8 to 14 dBm, $V_{RF\text{-}max}$ and $V_{m2\text{-}min}$ are very close to each other, with $V_{m2\text{-}min}$ always slightly larger than $V_{RF\text{-}max}$. This indicates that $V_{RF\text{-}max}$ can be tracked by checking $V_{m2\text{-}min}$ in this optical power range.

*Table 1: Measured $V_{RF\text{-}max}$ and $V_{m2\text{-}min}$ at different $P_{opt}$'s. The RF source frequency is 1 GHz.*

| $P_{opt}$ (dBm) | 4 | 6 | 8 | 10 | 12 | 14 |
|---|---|---|---|---|---|---|
| $V_{RF\text{-}max}$ (V) | 3.4 | 3.3 | 3.6 | 3.4 | 3.1 | 3.0 |
| $V_{m2\text{-}min}$ (V) | - | 3.9 | 3.7 | 3.5 | 3.3 | 3.1 |

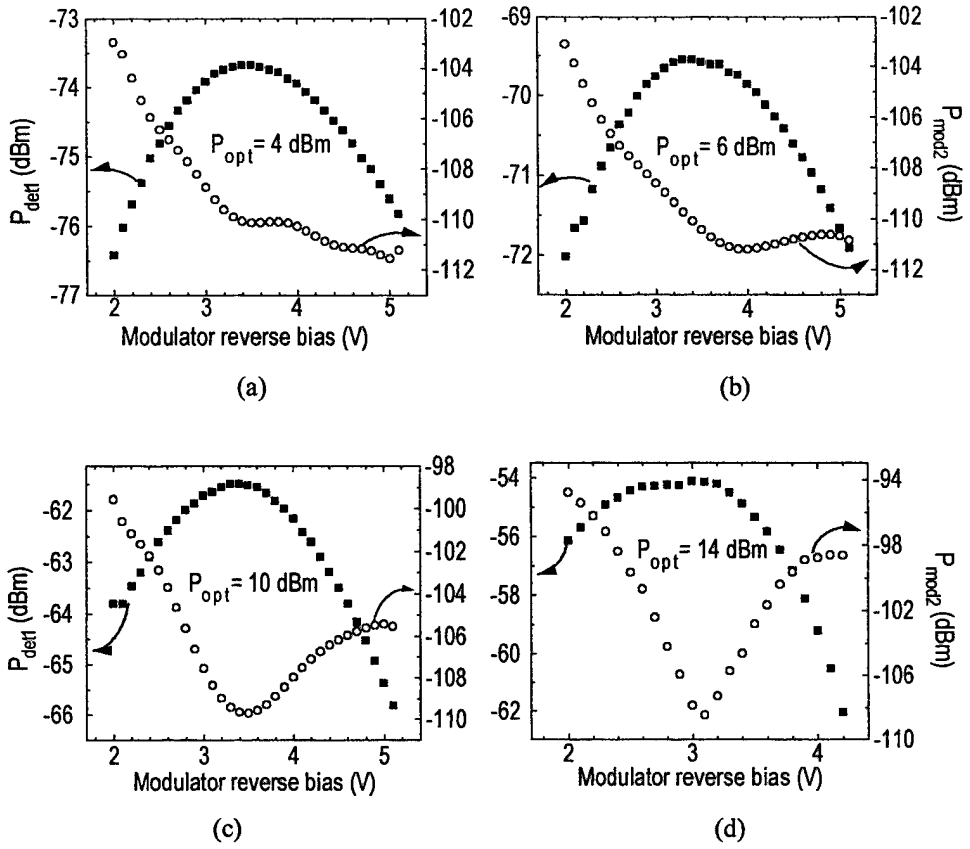


*Fig. 5. (a)-(d). Detector fundamental signals $P_{det1}$ (solid) and modulator second harmonic signals $P_{mod2}$ (open circle) as functions of modulator bias, at different $P_{opt}$'s. In each plot, the left y-axis is $P_{det1}$, the right y-axis is $P_{mod2}$. The RF loss between the source and the EAM is approximately 6 dB. The RF source frequency is 1 GHz.*

The above measurements are done at 1.32 μm wavelength with TE polarized light. Our measurements indicate that this bias tracking characteristic remains in place as the laser wavelength or the polarization is changed. Similar measurements have been done for another packaged EAM device, with TM polarized light and 750 MHz frequency RF source. The same bias-tracking characteristics have been observed.

***Analysis:*** The harmonic behavior of the EAM can be understood using circuit analysis. A simplified circuit depicting the connection to the EAM in the measurement set-up is shown in Fig. 6. The device parasitic effects are typically quite small and can be ignored at RF frequencies below 1 GHz.

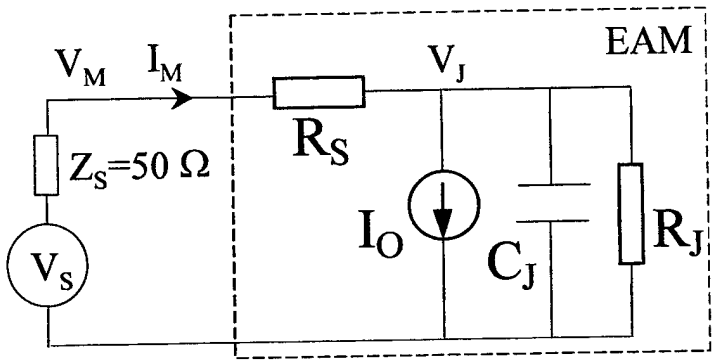


*Fig. 6. Equivalent circuit of the EAM transmitter. $I_O$ denotes the voltage dependent photocurrent. $Z_S$ represents either the source internal impedance for forward-going microwave, or the spectrum analyzer load impedance for the backward-going microwave.*

The voltage source $V_S$ includes both RF source and DC voltage source. $Z_S$ represents (1) the internal impedance of DC voltage source, (2) the internal impedance of RF source for forward-going microwave, (3) the sink impedance of isolator for backward-going fundamental signal, (4) the load impedance of spectrum analyzer for the backward-going second harmonic signal. The dashed region represents the lumped-element equivalent circuit of the EAM. In this model, $I_o$ is the voltage dependent photocurrent governed by the electroabsorption effect; $R_S$ is the series resistance from ohmic contacts and doped semiconductor layers; $C_J$ and $R_J$ are junction capacitance and resistance respectively, at junction voltage $V_J$. The EAM voltage and current are $V_M$ and $I_M$ respectively.

The second harmonic signal at $Z_S$ can be obtained by applying the harmonic balance method to the circuit. $I_M$, $V_J$, $V_M$ and $V_S$ include both DC ($I_{MO}$, $V_{JO}$, $V_{MO}$, and $V_{SO}$ respectively) and AC components. For instance $I_M$ can be expressed up to the second harmonic as:

$$I_M = I_{M0} + i_{m1}e^{j\omega t} + i_{m2}e^{j2\omega t} \qquad (7)$$

and likewise for $V_J$, $V_M$ and $V_S$. Note that $v_{s2}=0$ at the source. The circuit elements are related by:

$$I_M = I_O + \frac{d}{dt}(C_J V_J) + \frac{V_J}{R_J} \qquad (8)$$

$$V_M = I_M R_S + V_J \qquad (9)$$

$$V_S = V_M + I_M Z_S \qquad (10)$$

Since $C_J$ and $I_O$ depend on $V_J$, they can be approximated, using Taylor's expansion, as:

$$I_O = I_{O0} + I'_O v_{j1} e^{j\omega t} + (I'_O v_{j2} + I''_O v_{j1}^2) e^{j2\omega t} \quad (11)$$

$$C_J = C_{J0} + C'_J v_{j1} e^{j\omega t} + (C'_J v_{j2} + C''_J v_{j1}^2) e^{j2\omega t} \quad (12)$$

where primes denote derivatives of the DC component w.r.t. $V_{J0;}$ $v_{jk}$ is the $k^{th}$ harmonic of $V_J$. Balancing the DC parts in Eqs. (8) and (9), one gets:

$$\frac{dI_{M0}}{dV_{M0}} = \left(\frac{dI_{O0}}{dV_{J0}} + \frac{1}{R_J}\right)\left(1 - \frac{dI_{M0}}{dV_{M0}} R_S\right) \quad (13)$$

As we previously pointed out, when the optical power is below the saturation level, $V_{RF\text{-}max}$ is the bias for both maximum RF gain and maximum $I'_O = dI_{O0}/dV_{J0}$. If the $(dI_{M0}/dV_{M0})R_S$ term on the right side of Eq. (13) is << 1, $dI_{M0}/dV_{M0}$ will also be maximized around the same bias. For a typical EAM, $dI_{M0}/dV_{M0}$ is less than 10 mA/V, $R_S$ is usually less than 10 Ω, so that $(dI_{M0}/dV_{M0})R_S << 1$. This explains why the approach in Ref. [5] can work well for tracking the EAM bias.

By balancing the AC components of the same order in Eqs. (8) to (10), the fundamental signal voltage at the junction is:

$$v_{j1} = \frac{v_{s1}}{A(R_S + Z_S) + 1} \quad (14)$$

where A equals $I'_O + j\omega(C_{J0} + C'_J V_{J0}) + 1/R_J$; and the second harmonic voltage of the modulator is,

$$v_{m2} = -\frac{B_2 Z_S}{B_1(R_S + Z_S) + 1} v_{j1}^2 \quad (15)$$

where $B_1$ equals $I'_O + j2\omega(C_{J0} + C'_J V_{J0}) + 1/R_J$, $B_2$ equals $I''_O + j2\omega(C'_J + C''_J V_{J0})$. From Eqs. (14) and (15) we see that the second harmonic voltage $v_{m2}$ is proportional to the square of the fundamental signal voltage $v_{s1}$ of the RF source. This has been observed in our measurements when the RF source power was changed from –20 dBm to –15 dBm.

When the optical power is below the saturation value, both $I'_O$ and $I''_O$ increase with optical power with little dependence on RF frequency. After the EAM intrinsic region is fully depleted, $C_{J0}$ varies very little with $V_{J0}$, and thus $C'_J$ and $C''_J$ are very small. Consequently, with relatively high optical power and low RF frequency, the variations of

A, $B_1$ and $B_2$ with $V_{M0}$ are mainly due to the variations of $I_O'$ and $I_O''$. At DC bias $V_{RF-max}$, $I_O'$ is at maximum and $I_O''=0$, therefore A and $B_1$ are also close to their respective maximum and $|B_2|$ is close to its minimum. Inserting these results in Eqs. (14) and (15), it can be derived that $v_{m2}$ reaches a minimum at bias close to $V_{RF-max}$. The above analysis also implies that with a lower pilot tone frequency, $V_{m2-min} \approx V_{RF-max}$ begins at a lower $P_{opt}$. For example, with a 1 MHz pilot tone frequency, the optical power range for bias tracking of $V_{RF-max}$ by $V_{m2-min}$ can be extended to below 0 dBm.

For the case of no optical power, or for the case of low optical power and high RF frequency, the generation of the second harmonic at the EAM is mainly due to the variation of junction capacitance. The variation of $C_J$ with $V_J$ is smaller at higher EAM DC bias, so that in this case the EAM second harmonic decreases monotonically with bias. This effect of $C_J$ to second harmonic also makes $V_{m2-min}$ slightly larger than $V_{RF-max}$ in cases of high optical powers and low RF frequency.

The above modeling provides an intuitive understanding for the EAM harmonics, and it predicts the same trends as is obtained by measurement. To implement the proposed self-bias control scheme, the dithering RF signal (~1 MHz) and its harmonics can be applied and checked through the DC port of the broadband EAM bias-T. For this implementation, a bias-T with a DC to AC crossover frequency well above the dithering frequency must be employed. In this way, the EAM modulation bandwidth will not be affected by the required bandpass filters and the octave-band circulator.

In short, we have shown that over an optical power range, the second harmonic signal of the EAM exhibits a dip close to the bias point for maximum RF link gain. Using an equivalent circuit analysis we conclude this is due to the inherent electroabsorption effect in the modulator. The above phenomenon can be exploited for dynamic self-bias control for electroabsorption modulators for analog fiber-optic link applications. As $V_{RF-max}$ drifts due to changes in operating conditions, it can be tracked by determining the bias voltage, $V_{m2-min}$, where the second harmonic shows a dip. The analysis also suggests that a lower pilot tone frequency can extend the optical power range for bias tracking.

## C. A Concise RF Equivalent Circuit Model for Electroabsorption Modulators

A RF equivalent circuit model of EAMs based upon parameters that carry physical meaning and can be accurately measured can facilitate the design of EAM driver and the related RF link performance [8]. Since EAMs are inherently optoelectronic devices, its equivalent circuit model should also incorporate the optical effect. A small-signal equivalent circuit model for MQW EAMs has been proposed previously [9]. However, in the prior model, some empirical parameters are included which are not typical for other devices. The model treats the EAM as a photodetector (PD) that receives the modulated optical signal. Furthermore, this prior model has not been used in estimating the EAM frequency response. In this work, we present a new circuit model that removes these shortcomings and clarifies the effect of the optical power to the E/O response and device impedance.

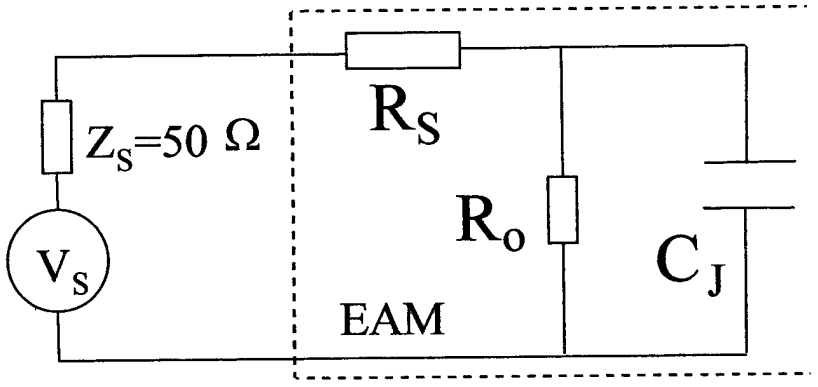


*Fig. 7. RF equivalent circuit model for a lumped EAM.*

***Model:*** The EAM photocurrent is the key issue in the present equivalent circuit model. Unlike the photocurrent in a PD, photocurrent in an EAM is represented as a current path, rather than as a current source. The impedance of this current path can be modeled by a resistance $R_o=(dI_o/dV_j)^{-1}$, where $I_o$ is EAM DC photocurrent and $V_j$ is the junction DC voltage. The resulting equivalent RF circuit model for the EAM is depicted in Fig. 7, where $C_J$ is the junction capacitance; $R_S$ is the device series resistance, including the ohmic contact resistance at the electrodes and the bulk resistance in the doped semiconductor layers. Parasitic capacitance (typically ~fF) and junction leakage resistance (usually ~MΩ) are ignored in this model. Parasitic inductance can be included

for packaged devices. The modulator E/O frequency response is determined from the ratio of AC voltage across $C_J$ to the input AC voltage to the modulator.

***Measurements:*** The measured EAM consists of 8 InAsP/GaInP QWs (8.9 nm compressively strained InAsP well and 7.4 nm tensile-strained GaInP barrier) absorption region grown on InP substrate. Doped InGaAsP waveguiding layers are added to improve the optical coupling efficiency to lensed fibers. The waveguide is 200 μm long and 3 μm wide. With TE polarized 1.32 μm wavelength light, an optical insertion loss at 9 dB is obtained at zero bias voltage; a maximum slope efficiency of 1.2 $V^{-1}$ is measured at - 0.7 V bias. A Lightwave Component Analyzer (HP8703A) is used to measure the $S_{11}$ and the modulator E/O response simultaneously. To investigate the optical power effect, measurements are performed at both 0 dBm and 10 dBm optical power.

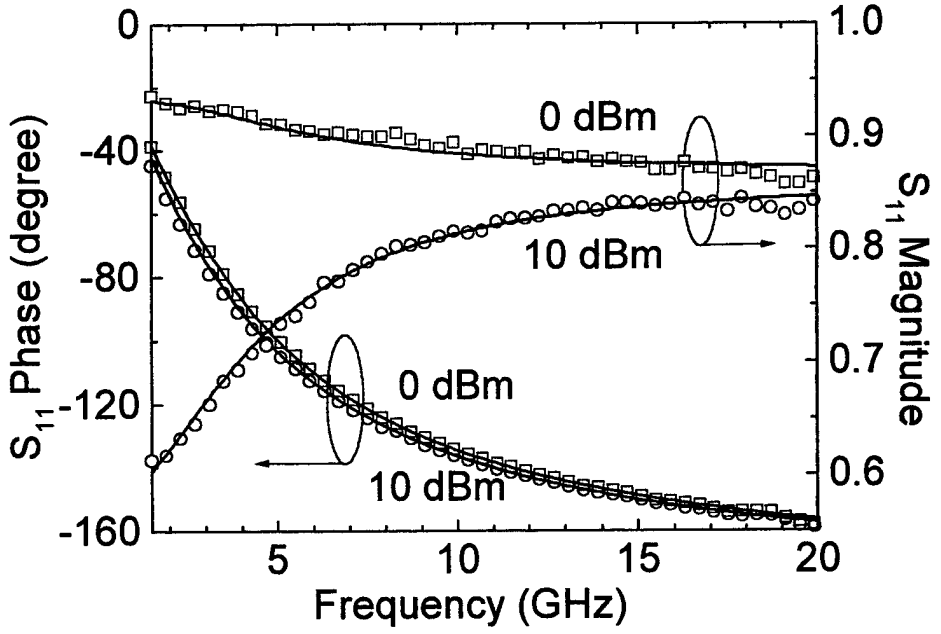


*Fig. 8. Measured (symbols) and calculated (solid lines) $S_{11}$ data for the MQW EAM at different optical powers.*

Fig. 8 plots the measured $S_{11}$ magnitude and phase values of the EAM (as symbols) at –0.7 V bias. Solid curves are the interpolated $S_{11}$ magnitudes and phases, using circuit parameters (listed in Table 1) extracted from measured $S_{11}$ values. The calculated $S_{11}$ phase curves almost coincide with the measured $S_{11}$ phase curves. When

the input optical power changes from 0 to 10 dBm, the $S_{11}$ phase changes slightly, while the magnitude changes significantly, especially at low frequencies. This is explained by the large reduction of the photocurrent resistance $R_o$, as shown in Table 1. At larger optical power, the photocurrent increases even faster with the junction voltage, resulting in a much smaller $R_o$. It is noted that the series resistance $R_S$ and junction capacitance $C_J$ change slightly with optical power, causing small modification to $S_{11}$.

Since the EAM photocurrent is related to the carrier transport process inside the intrinsic region of the diode, we anticipate the carrier escape time may affect the equivalent circuit model [10]. However, the carrier escape time can hardly affect low frequency signal; while at high frequencies, the capacitor $C_J$ has a relatively smaller impedance and dominates the frequency response. Ref. 2 suggested incorporating the carrier escape time effect with an inductive element. In our equivalent circuit analysis, we find that such an inductor is very small in value and thus causes a negligible effect to the calculated results. Further investigation will be needed to fully understand the effect of carrier escape time on the EAM equivalent circuit model.

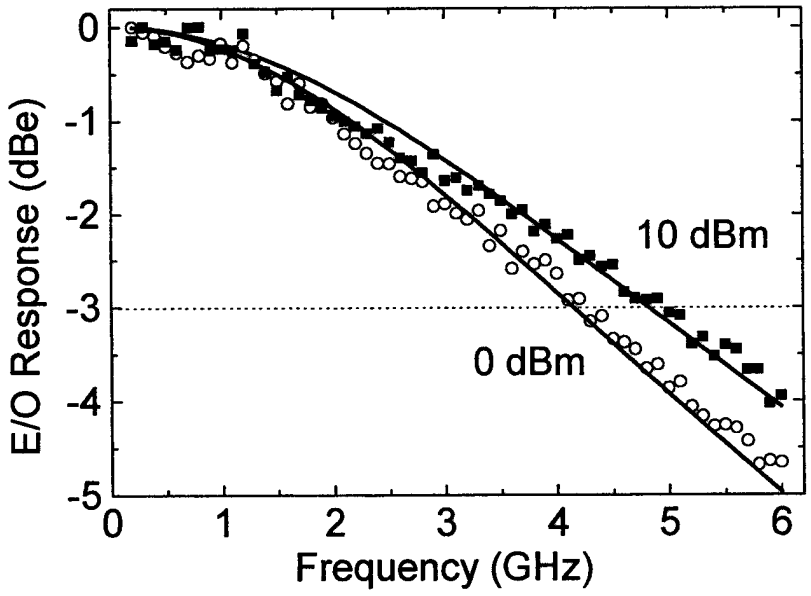


*Fig. 9. Measured (symbols) and calculated (solid lines) E/O responses for the MQW EAM at different optical powers.*

The measured modulator E/O responses at the two optical powers are plotted as symbols in Figure 9. Using parameters from Table 2 we obtain the calculated E/O response (solid) curves shown in the same figure. A good agreement between the measured data and the calculated curves is observed. According to our model, the modulation bandwidth increases by ~ 0.6 GHz when the optical power increases from 0 to 10 dBm. This again is mainly attributed to the large reduction of $R_o$, which reduces the effective RC time constant. The low frequency RF gain due to the modulator E/O conversion increases from –37.7 to –20.8 dB as the optical power is increased from 0 to 10 dBm. This represents a 3.1 dB RF gain compression at 10 dBm optical power, ~2 dB of which is contributed from the reduction of $R_o$, while the remaining 1 dB is attributed to the carrier screening effect.

*Table 2: Extracted circuit parameters for the MQW EAM at different optical powers.*

| Optical Power | $R_S$ (Ω) | $C_J$ (pF) | $R_o$(Ω) |
|---|---|---|---|
| 0 dBm | 3.6 | 0.77 | 1400 |
| 10 dBm | 3.8 | 0.81 | 180 |

In short, in this program we have developed a concise RF equivalent circuit model for EM modulatiors using only three physical circuit parameters. This model has demonstrated excellent agreement with observed E/O response and is consistent with EAM impedance consideration.

## D. Integrated Electroabsorption Waveguide and Mixer for Frequency Conversion

Frequency converting photonic links for antenna remoting applications is a good application where antenna front-end hardware complexity can be minimized and the deleterious effects of fiber dispersion may be avoided [11]. Many of the conversion schemes take advantage of the optical local oscillator (LO), which is less complex than the electronic LO at high frequency, and has shown lower phase noise. There have been several proposals to achieve low conversion loss and large spur-free dynamic range (SFDR) for photonic frequency converting links [12-14]. One approach makes use of

Mach-Zehnder modulators at very high optical LO power (350 mW) to achieve positive link conversion gain (defined as the ratio of the output converted RF power to the input RF power) [14].

In this project, a new RF signal conversion approach is proposed and demonstrated using an electroabsorption (EA) waveguide as a photodetector/mixer. Unlike previous approaches, frequency converted electrical RF signals from the EA waveguide, operating as an optoelectronic mixer (OEM), are generated and made available for subsequent signal processing. This converted RF signal can be sent through conventional electrical cable that has low attenuation at baseband/IF frequency. This avoids using high LO power to compensate the fiber RF link loss. We have demonstrated a moderate conversion loss and high SFDR RF signal mixing using moderate optical LO power and a simple system configuration.

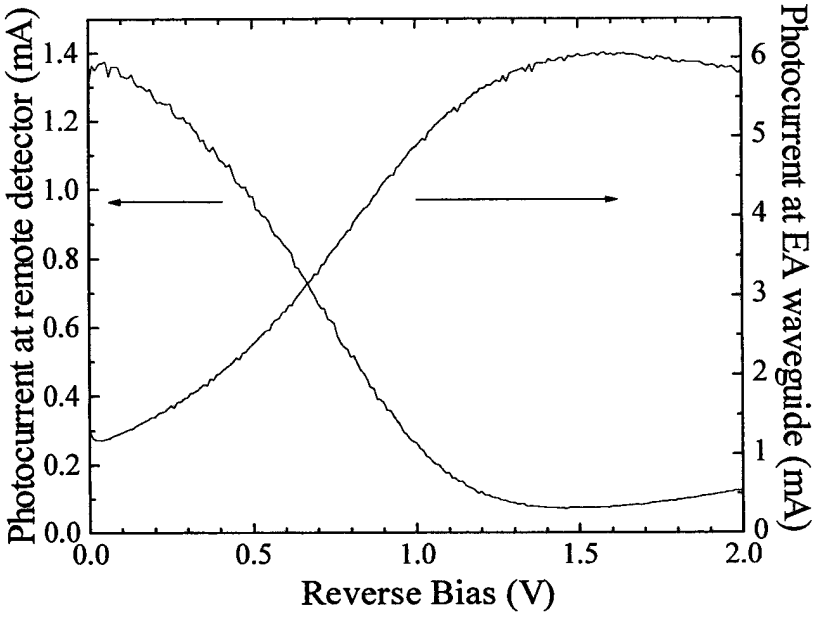


*Fig. 10. Transmission (photocurrent at remote detector) and absorption (photocurrent at modulator) characteristics of the MQW EA waveguide used. Optical power is 10 mW at 1.319 μm.*

When optical power is incident on EA waveguides, the electroabsorption process generates an electric-field-dependent photocurrent, $I_{ph}$, expressed as

$I_{ph}(V, P_{opt}) = \eta_m(V) P_{opt}$, where $P_{opt}$ is the optical power and $\eta_m(V)$ is the modulator's detection responsivity. As depicted in Fig. 10, $\eta_m$ is dependent on the applied bias (therefore, the electric field), and is independent of optical power provided that the device is operated below saturation.

When a DC optical power, $P_0$, and modulated optical power, $p$ at $\omega_{LO}$, are incident on an EA waveguide driven by a DC bias voltage, $V_b$, along with a RF signal voltage, $v$ at $\omega_s$, the device photocurrent is given by:

$$I_{ph}(V, P_{opt}) = \eta_m(V_b + v\cos\omega_s t) \cdot (P_0 + p\cos\omega_{LO} t) \qquad (16)$$

Using a small signal analysis of $\eta_m(V_b + v\cos\omega_s t)$, the up-and down-converted signals at $\omega_s \pm \omega_{LO}$ are obtained as:

$$I_{ph}^{mix} = \frac{1}{2}\frac{d\eta_m}{dV}\bigg|_{Vb} vp\cos(\omega_s \pm \omega_{LO})t, \qquad (17)$$

where $\frac{d\eta_m}{dV}\Big|_{Vb}$ is the first-order derivative evaluated at the DC bias voltage. The higher order derivatives of $\eta_m$ will contribute to the harmonic and intermodulation distortions of this OEM. Note from $\frac{d\eta_m}{dV}\Big|_{Vb}$ in (17) that the electro-absorption is crucial in generating mixed signals. This distinguishes the EA waveguides in the detector mode [15] from the usual *pin* photodetector that is biased to give a *constant responsivity with voltage.*

In this work, we compare the current that gives the mixed signals detected by the remote detector, when the EAM is used as a modulator. The current detected by the remote detector can be expressed as $I_{trans} = \eta_d P_{opt} t_{ff} T(V)$, where $\eta_d$ is the responsivity of the remote detector, $t_{ff}$ is the transmission factor of the EAM, and $T(V)$ is the transfer function of the EAM normalized to the incident optical power. The corresponding photocurrent that gives the mixing of $\omega_s$ and $\omega_{LO}$ is:

$$I_{trans}^{mix} = \frac{1}{2}\eta_d t_{ff}\frac{dT}{dV}\bigg|_{Vb} vp\cos(\omega_s \pm \omega_{LO})t. \qquad (18)$$

From $I_{ph}^{mix}$ with $I_{trans}^{mix}$, the RF power of the converted signals can be calculated, assuming 50-Ω load resistor dissipating the RF power. The ratio of powers of the frequency conversion signals in these two cases can be calculated in dB as:

$$Ratio = 20Log\left(\frac{I_{ph}^{mix}}{I_{trans}^{mix}}\right), \tag{19}$$

which can be expressed with DC transfer curve parameters as follows:

$$Ratio = 20Log\left(\frac{dI_{ph}/dV}{dI_d/dV}\right). \tag{20}$$

Here $I_{ph}$ and $I_d$ are the DC photocurrent detected at the EAM and remote detector, respectively, and the derivatives are evaluated at the operating bias, $V_b$.

In the experiments, an anti-reflection coated strain-compensated InAsP/GaInP multiple-quantum-well (MQW) EA waveguide that utilizes the quantum-confined Stark effect (QCSE) was used [16]. The undoped electroabsorption layer was composed of 8 periods of 8.9-nm thick compressively-strained InAsP wells and 7.4-nm thick tensile-strained GaInP barriers, sandwiched by InGaAsP cladding layers. At an optical power of 10 mW ($\lambda$ = 1.319 μm), the transmission (as detected by a remote detector with 0.89-A/W responsivity) and device photocurrent characteristics vs. DC bias of this EA waveguide are shown in Fig. 10. The normalized slope efficiency is -1.1 $V^{-1}$ for the transmission curve. The fiber-to-fiber insertion loss of this waveguide as a modulator was estimated to be 8.0 dB. The electrical 3-dB bandwidth of this device was separately measured to be 4.8 GHz without using a 50-Ω matching resistor. The length of this waveguide device was 185 μm.

The RF frequency mixing experiment was set up as shown in Fig. 11. Two Nd:YAG lasers were set up to generate a beat tone at 900 MHz with 100-% modulation depth, which was used as an optical LO signal to the EA waveguide OEM. Electrical voltage that contained the DC bias as well as the RF signal at $\omega_s$ = 1.0 GHz was applied to the device. The DC bias used was –0.75 V, which corresponds to the highest slope efficiency of the photocurrent vs. DC bias curve. A RF circulator (bandwidth 1~2 GHz)

was inserted between the device under test and the RF spectrum analyzer to measure the RF power generated at the device.

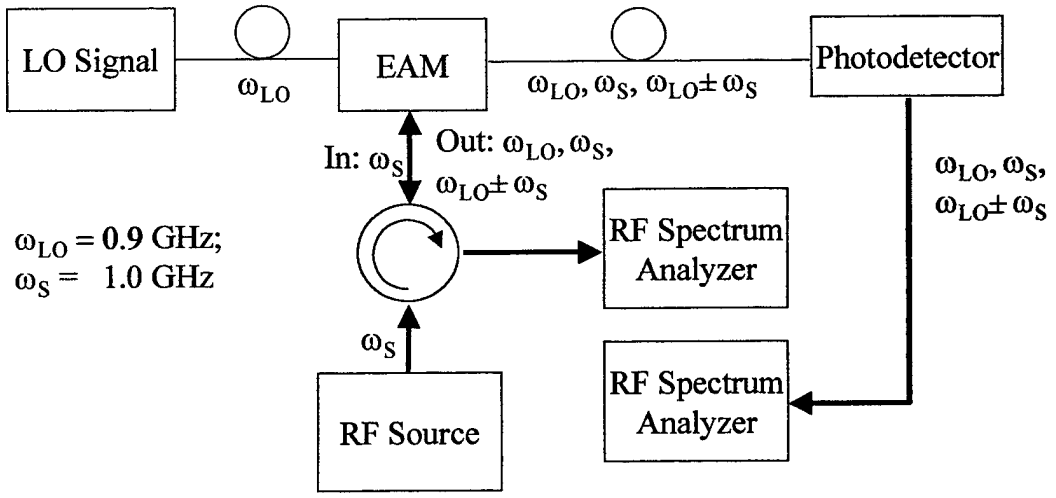


*Fig. 11. Experimental set-up for the mixing experiment using the EA waveguide.*

Fig. 12 summarizes the measured RF signals from the EA waveguide converter. The optical LO power incident on the EA waveguide was 10 mW, and the input RF power was –20 dBm. The LO was observed at 900 MHz, and the signal at 1.0 GHz. Up-converted signal power detected at 1.9 GHz was –38.9 dBm after calibration of the microwave loss due to the cables. In Fig. 12, other RF signals are also evident, e.g., second harmonics of the LO at 1.8 GHz; down-converted signal at 0.1 GHz; third-order intermodulation distortions ($IMD_3$) of the LO and the RF signal at 0.8 GHz, etc. The up- and down-converted signals appear to have different RF power, caused by the bandwidth limitation of the circulator. When the RF signal power was increased to –10 dBm, the converted signal powers increased by 10 dB. They closely follow the behavior predicted by (2). It was also found that the device became saturated around 10-mW LO optical power. Compared with the measurement at low optical power (1 mW), the RF link gain comprised of this EA waveguide as an external modulator was compressed by 4 dB at 10 mW.

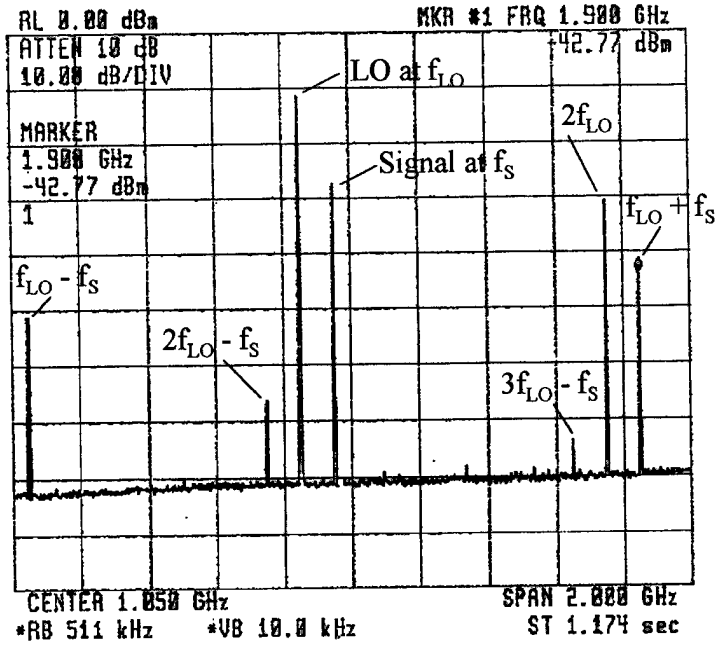


*Fig. 12. Measured RF spectrum at the EA waveguide.*

We have also measured the RF power transmitted through the fiber and detected by the remote detector. It has a similar RF spectrum as Fig. 12, but due to the link loss, the original signal power at $\omega_s$ is attenuated (link loss = 21 dB). Up-converted signals are now measured to be –48.8 dBm. (After microwave-loss calibration, the power becomes –47.8 dBm.) Up- and down-converted signals are observed to have the same power. When we measure the mixing using an increased signal power –10 dBm from –20 dBm, the converted signal powers increase by 10 dB, which closely follows the behavior predicted by Eq.18.

Defining the conversion loss as the ratio of the input RF signal power to the output converted signal power, the conversion loss for the case when the EA waveguide was used as a photodetector/mixer is found to be 18.9 dB. The conversion loss obtained above is mainly limited by LO optical power and the saturation power of the EA waveguide used. It could be improved by using an EA waveguide with higher saturation. Increasing the LO power can increase the converted RF power, as shown in Eq. 17.

Decreasing the coupling loss from the fiber to the EA waveguide is another approach, which also increases $\eta_m$. When this EA waveguide was used as a modulator/mixer and the converted signals were transmitted through the optical fiber as in [12-14], the conversion loss was increased to 27.8 dB. The increase in conversion loss (8.9 dB) is mainly due to the fact that the responsivity of the remote detector, $\eta_d$ at the end of the fiber link combined with the EA waveguide insertion loss, $t_{ff}$, was much smaller than that of the EA waveguide, $\eta_m$, i.e., $t_{ff}\eta_d < \eta_m$.

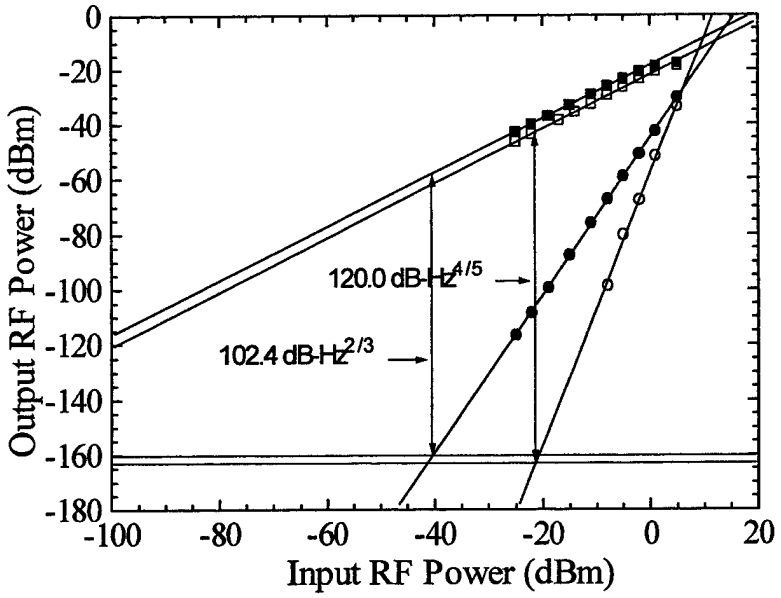


*Fig. 13. Two-tone test of the MQW EA photodetector/RF mixer. Converted RF signals (■: for highest slope point, □: for third-order null point) and the $IMD_3$'s (●: for highest slope point, ○: third-order null point) are shown. Noise floors (dotted lines) were dominated by the shot noise and given by –160 dBm/Hz and –163 dBm/Hz for the highest slope point and the third-order null point, respectively.*

The two-tone SFDR of the EA waveguide photodetector/RF mixer was also measured, as shown in Fig. 13. With two RF tones at 1.00 and 1.02 GHz and the optical LO tone at 0.90 GHz, the converted signals and the their $IMD_3$'s were measured. (Due to the bandwidth limitation of the circulator, only the up-converted signals were measured.) When the EA waveguide was biased at the highest slope point of the device photocurrent

vs. DC bias curve (second-order null point), a SFDR of 102.4 dB-$Hz^{2/3}$ was obtained at 10-mW optical LO power for the up-converted signal at 1.90 GHz. The noise floor was dominated by the shot noise due to the device photocurrent. When the EA waveguide was biased at the third-order null point of the device photocurrent vs. DC bias curve (0.44 V), the up-converted RF signal power was reduced by ~3 dB, but the suboctave SFDR was measured at 120.0 dB-$Hz^{4/5}$ with the fifth-order dependence on the input RF power. At the third-order null point, the $IMD_3$ due to the third-order input power dependence becomes null, making the $IMD_3$ depending on the next order, which is the fifth order.

A bulk InGaAsP-InP EA waveguide that uses the Franz-Keldysh effect was also tested for RF signal conversion. The transmission characteristic of the Franz-Keldysh EA device is shown in Fig. 14. Larger RF conversion loss (29.2 dB) was measured when this EA waveguide was used as a photodetector/mixer at the same LO optical power of 10 mW, than those obtained with MQW waveguides. This result is mainly due to the smaller slope efficiency (0.18 $V^{-1}$) of the bulk EA waveguide and demonstrates the importance of the slope efficiency of the EA waveguide when it is utilized as a photodetector/mixer.

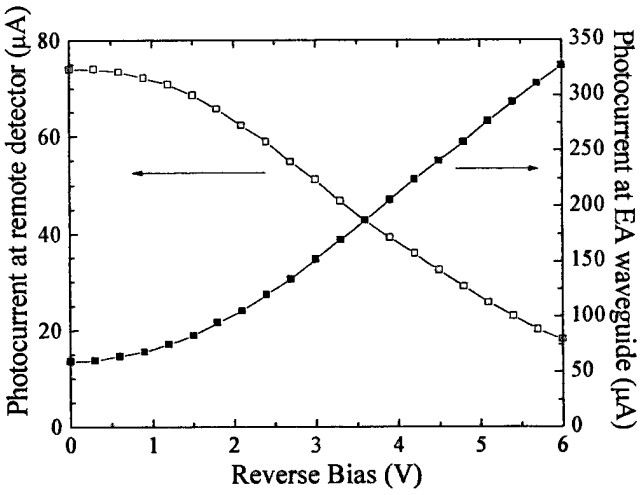


*Fig. 14. Transmission (photocurrent at remote detector) and absorption (photocurrent at modulator) characteristics of the Franz-Keldysh EA waveguide for an optical power of 1 mW at 1.319 μm. Fiber-to-fiber insertion loss was 10.7 dB.*

In short, we have demonstrated that the MQW EA waveguide can be utilized as an OEM that combines both functions of a electroabsorption photodetector and an electronic mixer. It has been pointed out that the slope efficiency of the EA waveguide is extremely important in determining conversion gain. Currently 18.9 dB conversion loss has been obtained and this result can be reduced with higher optical power. This scheme can be useful in antenna applications where optical LO signal distribution is used for frequency converting microwave signals.

## References


1. Ido, T.; Tanaka, S.; Koizumi, M.; Inoue, H.: "Ultra-high-speed MQW electroabsorption modulators with integrated waveguides", Proceedings of the SPIE - The International Society for Optical Engineering, vol.3006, (Optoelectronic Integrated Circuits, San Jose, CA, USA, 12-14 Feb. 1997.) p.282-90
2. Liao, H.H.; Mei, X.B.; Loi, K.K.; Tu, C.W.; Asbeck, P.M.; Chang, W.S.C., "Microwave structures for traveling-wave MQW electro-absorption modulators for wide band 1.3 μm photonic links", Proceedings of the SPIE - The International Society for Optical Engineering, vol.3006, (Optoelectronic Integrated Circuits, San Jose, CA, USA, 12-14 Feb. 1997.) p.291-300.
3. Kawano, K.; Kohtoku, M.; Ueki, M.; Ito, T.; Kondoh, S.; Noguchi, Y.; Hasumi, Y.: "Polarisation-insensitive travelling-wave electrode electroabsorption (TW-EA) modulator with bandwidth over 50 GHz and driving voltage less than 2 V," Electronics Letters, vol.33, (no.18), Aug. 1997. P.1580-1.
4. M. M. Mihailidi, IEEE Microwave and Optical Technol. Letts., vol.10, p.204-7, 1995.
5. Li, G.L.; Welstand, R.B.; Chen, W.X.; Zhu, J.T.; Pappert, S.A.; Sun, C.K.; Liu, Y.Z.; Yu, P.K.L.: "Novel bias control of electroabsorption waveguide modulator", IEEE Photonics Technology Letters, vol.10, (no.5), May 1998. P.672-4
6. Loi, K.K.; Mei, X.B.; Hodiak, J.H.; Tu, C.W.; Chang, W.S.C.: "38 GHz bandwidth 1.3 μm MQW electroabsorption modulators for RF photonic links", Electronics Letters, vol.34, (no.10), May 1998. P.1018-19.
7. Spickermann, R.; Sakamoto, S.R.; Dagli, N.: "GaAs-AlGaAs traveling wave electro-optic modulators", Proceedings of the SPIE - The International Society for Optical Engineering, vol.3006, (Optoelectronic Integrated Circuits, San Jose, CA, USA, 12-14 Feb. 1997.) p.272-9.
8. Ramdane, A., Ougazzaden, A., Devaux, F., Delorme, F., Schneider, M., Landreau, J.: 'Very simple approach for high performance DFB laser-electroabsorption modulator monolithic integration', *Electron. Lett.*, 1994, **30**, pp. 1980-1981.
9. Metzler, G., and Schwander, T.: 'RF small-signal equivalent circuit of MQW InGaAs/InAlAs electroabsorption modulator', *Electron. Lett.*, 1997, **33**, (21), pp. 1822-1823.

10. Ido, T., Sano, H., Tanaka, S., and Inoue, H.: 'Frequency-domain measurement of carrier escape times in MQW electro-absorption optical modulators', *IEEE Photonics Technol. Lett.,* 1995, 7, (12), pp. 1421-1423.
11. G. K. Gopalakrishnan, R. P. Moeller, M. M. Howerton, W. K. Burns, K. J. Williams, and R. D. Esman, *IEEE Trans. Microwave Theory Tech.*, vol. 43, pp. 2318-2323, 1995.
12. C. K. Sun, R. J. Orazi, and S. A. Pappert, *IEEE Photon. Technol. Lett.*, vol. 8, pp. 154-156, 1996.
13. R. Helkey, J. C. Twinchell, and C. H. Cox, *J. Lightwave Technol.*, vol. 15, pp.956-961, 1997.
14. H. Roussell, R. Helkey, *IEEE Microwave Guided Wave Lett.*, vol. 8, pp. 408-410, 1998.
15. R. B. Welstand, S. A. Pappert, C. K. Sun, J. T. Zhu, Y. Z. Liu, and P. K. L. Yu, *IEEE Photon. Technol. Lett.*, vol. 8, pp. 1540-1562, 1996.
16. K. K. Loi, J. H. Hodiak, W. B. Mei, C. W. Tu, W. S. C. Chang, D. T. Nichols, L. J. Lembo, and J. C. Brock, *IEEE Photon. Technol. Lett.*, vol. 10, pp. 1572-1574, 1998.

## Publications sponsored by this contract

1. G. L. Li, R. B. Welstand, J. T. Zhu, and P. K. L. Yu, "Self-Bias Control of Electroabsorption Waveguide Modulator," Digest of 1998 IEEE International Microwave Symposium , Vol. 2, pp. 1007-1010 (1998).
2. R. B. Welstand, S. A. Pappert, D. T. Nichols, L. J. Lembo, Y. Z. Liu, and P. K. L. Yu, "Enhancement in Electroabsorption Waveguide Modulator Slope Efficiency at High Optical Power", IEEE Photonics Technology Letters, Vol. 10, No. 7, pp. 961-963, 1998.
3. D. S. Shin, C. K. Sun, W. X. Chen, S. A. Pappert, J. T. Zhu, R. Nguyen, Y. Z. Liu, and P. K. L. Yu, "A Novel structure for Dual-function Electroabsorption Waveguide Modulator/Phototransistor", Proc. SPIE, Vol. 3463, pp. 20-30 (1998).
4. D. S. Shin, C. K. Sun, W. X. Chen, S. A. Pappert, J. T. Zhu, R. Nguyen, Y.Z. Liu, and P. K. L. Yu, "A Novel structure for Dual-function Electroabsorption Waveguide Modulator/Phototransistor," Proc. SPIE, Vol. 3463, pp. 66-69 (1998).
5. P. K. L. Yu, J. T. Zhu, W. X. Chen, G. L. Li, R. B. Welstand, S. A. Pappert, C. K. Sun, R. Nguyen, and Y. Z. Liu, "Laser/Modulator module for analog fiber optic links", Proc. SPIE, Vol. 3547, pp. 37 – 44 (1998).
6. P. K. L. Yu, W. S. C. Chang, P. Asbeck, R. B. Welstand, K. K. Loi, H. H. Liao, G. L. Li, W. X. Chen, J. T. Zhu, S. A. Pappert, C. K. Sun, R. Nguyen, Y. Z. Liu, "Electroabsorption Waveguide Modulators for High Performance Analog Fiber Links", Digest of Microwave Photonics Conference, MWP'98 (Paper MC1) (1998).
7. G. L. Li, Y. Z. Liu, R. B. Welstand, C. K. Sun, W. X. Chen, J. T. Zhu, S. A. Pappert, and P. K. L. Yu, "Harmonic Signals from Electroabsorption Modulator and Its Application to Dynamic Modulator Bias Control", IEEE Photonics Technology Letts. Vol 11, pp. 659-661 (1999).

8. C. K. Sun, R. Nguyen, S. A. Pappert, G. L. Li, W. X. Chen, H. Jiang, and P. K. L. Yu, "Impedance Tuned EHF Electroabsorption Modulator for Narrowband Analog Fiber Optic Links", Proceedings of PSAA-9, Section on Photonic Systems for Antenna Applications (1999).
9. G. L. Li, W. X. Chen, P. K. L. Yu, C. K. Sun, and S. A. Pappert, "Ultra High-Speed Traveling Wave EAM: Design and Analysis", Proceedings of PSAA-9, Section on Photonic Systems for Antenna Applications (1999).
10. G. L. Li, W. X. Chen, P. K. L. Yu, C. K. Sun, and S. A. Pappert, "The Effects of Photocurrent on Microwave Properties of Electroabsorption Modulators", IEEE International Microwave Symposium, IMS'99 Digest, (1999).
11. G. L. Li, C. K. Sun, S. A. Pappert, W. X. Chen, and P. K. L. Yu, "Ultra High-Speed Traveling Wave Electroabsorption Modulator: Design and Analysis", IEEE Trans. MTT , Vol. 47, No. 7, pp. 1177-1183, 1999.
12. D. S. Shin, G. L. Li, C. K. Sun, S. A. Pappert, K. K. Loi, W. S. C. Chang, and P. K. L. Yu, "Optoelectronic RF Signal Mixing Using an Electroabsorption Waveguide as an Integrated Photodetector/Mixer", IEEE Photonics Tech. Lett. **12**(2), 193-195, 2000.
13. G. L. Li, D. S. Shin, W. S. C. Chang, P. M. Asbeck, P. K. L. Yu, C. K. Sun, S. A. Pappert, and R. Nguyen, "Design and Fabrication of Traveling Wave Electroabsorption Modulator", *SPIE Proceedings*, **Vol. 3950**, 2000.

## Presentations sponsored by this contract

1. G. L. Li, R. B. Welstand, J. T. Zhu, and P. K. L. Yu, "Self-Bias Control of Electroabsorption Waveguide Modulator," Presented at the 1998 IEEE International Microwave Symposium , Baltimore, June, 1998.
2. D. S. Shin, C. K. Sun, W. X. Chen, S. A. Pappert, J. T. Zhu, R. Nguyen, Y. Z. Liu, and P. K. L. Yu, "A Novel structure for Dual-function Electroabsorption Waveguide Modulator/Phototransistor", presented at the SPIE symposium, San Diego, July 1998.
3. D. S. Shin, C. K. Sun, W. X. Chen, S. A. Pappert, J. T. Zhu, R. Nguyen, Y.Z. Liu, and P. K. L. Yu, "A Novel structure for Dual-function Electroabsorption Waveguide Modulator/Phototransistor," presented at the SPIE symposium, San Diego, July 1998.
4. P. K. L. Yu, J. T. Zhu, W. X. Chen, G. L. Li, R. B. Welstand, S. A. Pappert, C. K. Sun, R. Nguyen, and Y. Z. Liu, "Laser/Modulator module for analog fiber optic links", presented at Photonics China 98 at Beijing, 1998. (Invited Presentation).
5. P. K. L. Yu, W. S. C. Chang, P. Asbeck, R. B. Welstand, K. K. Loi, H. H. Liao, G. L. Li, W. X. Chen, J. T. Zhu, S. A. Pappert, C. K. Sun, R. Nguyen, Y. Z. Liu, "Electroabsorption Waveguide Modulators for High Performance Analog Fiber Links", presented at the Microwave Photonics Conference, MWP'98 (Paper MC1) at Princeton, New Jersey (1998).
6. P. K. L. Yu, W. S. C. Chang, and Peter Asbeck, "Electroabsorption Modulator for High Performance Analog Fiber Links" presented at the RFLICS workshop, Crystal City, Virginia, January, 1999.
7. C. K. Sun, R. Nguyen, S. A. Pappert, G. L. Li, W. X. Chen, H. Jiang, and P. K. L. Yu, "Impedance Tuned EHF Electroabsorption Modulator for Narrowband Analog Fiber

Optic Links", Presented at the PSAA-9, Section on Photonic Systems for Antenna Applications Monterey, 1999.
8. G. L. Li, W. X. Chen, P. K. L. Yu, C. K. Sun, and S. A. Pappert, "Ultra High-Speed Traveling Wave EAM: Design and Analysis", Presented at the PSAA-9, Section on Photonic Systems for Antenna Applications Monterey, 1999.
9. G. L. Li, W. X. Chen, P. K. L. Yu, C. K. Sun, and S. A. Pappert, "The Effects of Photocurrent on Microwave Properties of Electroabsorption Modulators", IEEE International Microwave Symposium, Presented at the 1999 IEEE International Microwave Symposium , Anaheim, June, 1999).
10. G. L. Li, D. S. Shin, W. S. C. Chang, P. M. Asbeck, P. K. L. Yu, C. K. Sun, S. A. Pappert, and R. Nguyen, "Design and Fabrication of Traveling Wave Electroabsorption Modulator", Presented at SPIE Photnics West, San Jose, January, 2000.

**Dissertation sponsored by this contract**

"High Linearity Modulation and Detection in Semiconductor Electroabsorption Waveguides" by R. B. Welstand, Ph.D was awarded in 1998 at UCSD.

"Planar Photonic Devices using Surface Thin-film Stressors and Ion Implantation Isolation Techniques," by Q. Z. Liu, Ph. D was awarded in 1998 at UCSD.

**Acknowledgments**

The work reported here is mainly supported by the DARPA/AFRL program. Additional fundings are obtained from AASERT program, the California MICRO program, Raytheon, and SBIR programs through Fermionics Lasertech. We would like to acknowledge the technical collaboration with Dr. S. Pappert and Dr. C. K. Sun of NCCOSC of Point Loma, California.

# DISTRIBUTION LIST

| addresses | number of copies |
|---|---|
| AIR FORCE RESEARCH LABORATORY/SNDP<br>JAMES HUNTER<br>25 ELECTRONIC PKY<br>ROME NY 13441-4515 | 10 |
| UNIVERSITY OF CALIFORNIA SAN DIEGO<br>CONTRACT & GRANT ADMIN 0934<br>LA JOLLA CA 92093-0934 | 5 |
| AFRL/IFOIL<br>TECHNICAL LIBRARY<br>26 ELECTRONIC PKY<br>ROME NY 13441-4514 | 1 |
| ATTENTION: DTIC-OCC<br>DEFENSE TECHNICAL INFO CENTER<br>8725 JOHN J. KINGMAN ROAD, STE 0944<br>FT. BELVOIR, VA 22060-6218 | 1 |
| DEFENSE ADVANCED RESEARCH<br>PROJECTS AGENCY<br>3701 NORTH FAIRFAX DRIVE<br>ARLINGTON VA 22203-1714 | 1 |
| ATTN: NAN PFRIMMER<br>IIT RESEARCH INSTITUTE<br>201 MILL ST.<br>ROME, NY 13440 | 1 |
| AFIT ACADEMIC LIBRARY<br>AFIT/LDR, 2950 P.STREET<br>AREA B, BLDG 642<br>WRIGHT-PATTERSON AFB OH 45433-7765 | 1 |
| AFRL/MLME<br>2977 P STREET, STE 6<br>WRIGHT-PATTERSON AFB OH 45433-7739 | 1 |

AFRL/VACS/SURVIAC
2130 EIGHTH STREET, BLDG 45, STE 1
WRIGHT-PATTERSON AFB OH 45433-7542 1

AFRL/HESC-TDC
2698 G STREET, BLDG 190
WRIGHT-PATTERSON AFB OH 45433-7604 1

ATTN: SMDC IM PL
US ARMY SPACE & MISSILE DEF CMD
P.O. BOX 1500
HUNTSVILLE AL 35807-3801 1

TECHNICAL LIBRARY D0274(PL-TS)
SPAWARSYSCEN
53560 HULL ST.
SAN DIEGO CA 92152-5001 1

COMMANDER, CODE 4TL000D
TECHNICAL LIBRARY, NAWC-WD
1 ADMINISTRATION CIRCLE
CHINA LAKE CA 93555-6100 1

CDR, US ARMY AVIATION & MISSILE CMD
REDSTONE SCIENTIFIC INFORMATION CTR
ATTN: AMSAM-RD-OB-R, (DOCUMENTS)
REDSTONE ARSENAL AL 35898-5000 2

REPORT LIBRARY
MS P364
LOS ALAMOS NATIONAL LABORATORY
LOS ALAMOS NM 87545 1

ATTN: D'BORAH HART
AVIATION BRANCH SVC 122.10
FOB10A, RM 931
800 INDEPENDENCE AVE, SW
WASHINGTON DC 20591 1

AFIWC/MSY
102 HALL BLVD, STE 315
SAN ANTONIO TX 78243-7016 1

ATTN: KAROLA M. YOURISON
SOFTWARE ENGINEERING INSTITUTE
4500 FIFTH AVENUE
PITTSBURGH PA 15213 — 1

USAF/AIR FORCE RESEARCH LABORATORY
AFRL/VSOSA(LIBRARY-BLDG 1103)
5 WRIGHT DRIVE
HANSCOM AFB MA 01731-3004 — 1

ATTN: EILEEN LADUKE/D460
MITRE CORPORATION
202 BURLINGTON RD
BEDFORD MA 01730 — 1

OUSD(P)/DTSA/DUTD
ATTN: PATRICK G. SULLIVAN, JR.
400 ARMY NAVY DRIVE
SUITE 300
ARLINGTON VA 22202 — 1

AIR FORCE RESEARCH LAB/SND
25 ELECTRONIC PKY
ROME NY 13441-4515 — 1

TINA M. KNUTTI
AIR FORCE RESEARCH LAB/SNOR
25 ELECTRONIC PKY
ROME NY 13441-4515 — 1

ROBERT T. KEMERLEY
AIR FORCE RESEARCH LABORATORY/SND
2241 AVIONICS CIRCLE, RM C2G69
WRIGHT-PATTERSON AFB OH 45433-7322 — 1